Supplementary Information for

Uncovering hazards and adaptive capacity: A comprehensive risk assessment study in three conservation areas in Spain.

Rafael Mª NavarroCerrillo[1,2Ψ], Antonio Jesús Ariza-Salamanca[1Ψ]

[1]Department of Forest Engineering, Laboratory of Dendrochronology, Silviculture and Global Change, DendrodatLab-ERSAF, University of Cordoba, Campus de Rabanales, Crta. IV, km. 396, 14071 Córdoba, Spain.

[2]Instituto Interuniversitario del Sistema Tierra en Andalucía, Centro Andaluz de Medio Ambiente (IISTA-CEAMA), Avenida Mediterraneo, S/N, Granada 18006, Spain.

E-mail: rmnavarro@uco.es; telephone: +34-957-218657 fax: +34-957-218563

[Ψ]Equal contribution

This PDF file includes supplementary information and additional details of the article

CONTENTS

1. Description and additional details of the indicators used. 3
1.1. Exposed values 4
1.2. Hazard Magnitude 4
1.2.1. Fire Risk Index 4
1.2.2. Aridity Index 8
1.2.3. Pest and Disease Hazard 8
1.2.4. Forest continuity 9
1.2.5. Distance to roads 10
1.2.6. Population density 10
1.3. Susceptibility 10
1.3.1. Fuel load 10
1.3.2. Vertical forest continuity 11
1.3.3. Leaf Area Index 12
1.3.4. Flammability 12
1.3.5. Hydraulic traits 13
1.3.6. Rooting depth 14
1.3.7. Suppression difficulty index 15
1.4. Lack of Adaptative Capacity 18
1.4.1. Resprouting capacity 18
1.4.2. Seeding capacity 19
1.4.3. Evapotranspiration 20
1.4.4. Solar radiation 20
1.4.5. Slope 20
1.4.6. Forest management 20
1.5. Climatic scenarios 21
2. Weighting and aggregating the indicators 21
REFERENCES 24

1. Description and additional details of the indicators used.

The IPCC components of vulnerability and risk are exposed values, hazard magnitude, susceptibility and lack of adaptative capacity (Lecina-Diaz et al., 2021). Each component is defined by different indicators.

The indicators used and ancillary data are show in Table 1. All variables described below are freely accessible in the repository: https://doi.org/10.7910/DVN/FFVFCR

Cite dataset: Ariza-Salamanca, Antonio Jesús; Navarro-Cerrillo, Rafael M., 2023, "Replication Data for: Uncovering hazards and adaptive capacity: A comprehensive risk assessment study in three contrasted conservation areas in Spain", https://doi.org/10.7910/DVN/FFVFCR, Harvard Dataverse, V1

Format: GeoTIFF

Spatial resolution: 500 m

Coordinate Reference Systems: ETRS 89 UTM Zone 30N (25830) and REGCAN 95 UTM Zone 28N

Table 1. Selected indicators for each of the components of risk and vulnerability.

Component	Indicators
Exposed values	Carbon sink
Hazard magnitude	Fire Risk Index
	Aridity Index
	Pest and Disease Hazard
	Forest continuity
	Distance to roads
	Population density
Susceptibility	Fuel load
	Vertical forest continuity
	Leaf Area Index
	Flammability
	Hydraulic traits
	Rooting depth
	Suppression Difficulty Index
Lack of Adaptative Capacity	Resprouting capacity
	Seeding capacity
	Evapotranspiration
	Solar radiation
	Slope
	Forest management

1.1. Exposed values

Exposed values are the presence of ecosystem services that could be adversely affected by different disturbances (Lecina-Diaz et al., 2021). Here, we focused on the capacity of forests to store carbon. Carbon stocks (Biomass; Btot) is computed from aerial tree and shrubs biomass of each live individuals in each Spanish National Forest Inventory plots (Hereafter, IFN), that were computed from different dendrometric variables using species-specific allometric equations developed by Montero et al. (2005; 2020) for Spain.

The data consisted of a systematic sampling of permanent plots with a sampling density of one plot in every 1 km^2 of forest area, where trees above 7.5 cm were identified and measured within variable circular size plots (5 m radius for trees with DBH 7.5 cm, 10 m radius for trees with DBH 12.5 cm, 15 m radius for trees with DBH 22.5 cm and 25 m radius for trees with DBH 42.5). Shrub attributes were measured for circular, 10-m radius, sample plots. The IFN visually assesses mean height (decimeters; dm) and cover for each shrub species using a percentage scale with 1% interval widths.

The variable carbon sink (E) is defined as the change in biomass stock from the second (1986 - 1996) to the third IFN (1997 - 2007).

$$E = (BtotIFN3 - BtotIFN2)/10 \quad \text{(Eq.1)}$$

Unit: tons/ha·yr

We used the inverse distance weighting (IDW) to predict the value of the variable at an unsampled locations from the value of the variable at various sampled points.

We obtained the raw data of the second and third Spanish National Forest Inventory (IFN2 and IFN3; 1987 - 2007) in CSV format from the Ministry for Ecological Transition and Demographic Challenge (known by the abbreviation MITECO in Spanish) data repository (https://www.miteco.gob.es/es/biodiversidad/temas/inventarios-nacionales/inventario-forestal-nacional.html).

1.2.Hazard Magnitude

1.2.1. Fire Risk Index

We used the Fire Risk Index developed by the Andalusian Fight-Fighting Service (INFOCA). This index is based on an integrated approach in five areas: combustibility, topography, meteorology, historical and vulnerability. The risk obtained, arranged in five levels (low, moderate, high, very high and extreme). The general scheme followed for the calculation of the Fire Risk Index is shown below:

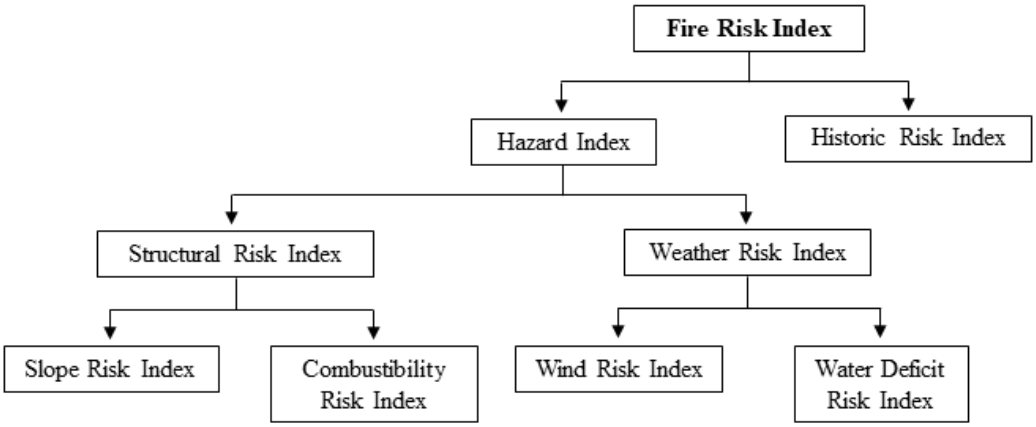

Figure 1. General scheme followed for the calculation of the Fire Risk Index.

To calculate each of the aggregate risk indices, a linear combination of the corresponding base indices was made, using coefficients with a value between 0 and 1, so as to assign a differentiated relative importance to each of the basic risk indices. This linear combination was then followed by a reclassification according to five risk categories.

Once both the Hazard Index (HI) and the Historic Risk Index (HRI) have been calculated, they have been combined to obtain the Fire Risk Index (FRI).

$$FRI = HI + 0.3 \cdot HRI \quad \text{(Eq.2)}$$

Unit: dimensionless

1.2.1.1.Hazard Index (HI)

This index reflects the probability of the fire spreading once it has started and is composed by the conjunction of two indices (structural and weather). The hazard index has been obtained as a linear combination of the structural risk index (SRI) and the weather risk index (WRI), with the following coefficients:

$$HI = SRI + 0.4 \cdot WRI \quad \text{(Eq.3)}$$

Structural Risk Index

The structural risk calculation integrates the slope and combustibility factors. The risk classification by slope that has been established for the calculation of structural risk is shown in the table below.

Table 2. Risk classification by slope.

Slope ranges (%)	Classification	Index value
0 - 10	Very low	1
10 - 20	Low	2
20 - 30	Medium	3
30 - 50	High	4

> 50	Very high	5

The risk due to the topography of the terrain has been calculated from the digital slope model available from the national centre for geographic information (https://centrodedescargas.cnig.es/CentroDescargas/catalogo.do?Serie=MDT02).

The risk classification by combustibility that has been established for the calculation of structural risk is shown in the table below.

Table 3. Risk classification by combustibility.

Fuel models	Classification	Index value
0	Very low	1
8, 5	Low	2
11, 9, 1, 3	Medium	3
7, 6, 2	High	4
4	Very high	5

Fuel models are based on Rothermel classification (Rothermel, 1972). For Sierra Nevada and Sierra de las Nieves National Parks, the risk due to combustibility has been calculated from the vector file of fuel models provided by Andalusian Environmental Information Network (https://portalrediam.cica.es/geonetwork/static/api/records/d0624371-78d7-4e89-b9ef-8e76a294bc97). For El Teide National Park, fuel models were provided by the Canary Islands government (https://opendata.sitcan.es/dataset/modelos-de-combustible-forestales-de-canarias).

Once both the slope risk index and the combustibility risk index have been calculated, they have been combined to obtain the structural risk index.

$$SRI = SRI + 0.5 \cdot CRI \quad \text{(Eq.4)}$$

Weather Risk Index

The second component of the Hazard Index corresponds to the weather risk index. This index reflects those factors related to meteorological conditions that will influence the development of the wildfire. These factors are wind speed and vegetation water deficit, which are assessed by means of the wind risk index (WNRI) and the water deficit risk index (WDRI) respectively.

The risk classification by wind that has been established for the calculation of weather risk is shown in the table below.

Table 4. Risk classification by wind speed.

Wind speed ranges (km/h)	Classification	Index value
< 30	Very low	1
30 - 50	Low	2
50 - 70	Medium	3
70 - 90	High	4
> 90	Very high	5

Average wind speed in raster format was downloaded from the Global Wind Atlas repository (https://globalwindatlas.info/es).

The water deficit risk index has been calculated as the ratio between precipitation and potential evapotranspiration (PET). The ranges considered for the calculation of the water deficit risk index were as follows:

Table 5. Risk classification by water deficit.

Water deficit ranges (mm)	Classification	Index value
> 1.08	Very low	1
1.08 – 0.81	Low	2
0.81 – 0.63	Medium	3
0.63 – 0.45	High	4
< 0.45	Very high	5

We obtained precipitation (P) raster data produced by the MITECO (https://www.miteco.gob.es/es/cartografia-y-sig/ide.html). Then, we applied a Thornthwaite-type water-balance model to calculate climatic water deficit (Thornthwaite, 1948; Hamon, 1963). Although various methods exist for computing water balance, Thornthwaite-type methods are most appropriate when data are limited to temperature and precipitation (Vörösmarty et al., 1998). Incorporating wind speed, humidity and net radiation (Penman, 1948) may improve the accuracy of the potential evapotranspiration (PET) calculation, but these data are rarely available in forest ecosystems.

The calculations of Thornthwaite (1948) are based on the determination of evapotranspiration as a function of average temperature, with a correction for photoperiod and number of days in the month. The method is widely used in the estimation of the water balance for climatology and climate classifications (see section 1.2.2., below). Temperature data for the calculation of potential evapotranspiration have been obtained from the MITECO (https://www.miteco.gob.es/es/cartografia-y-sig/ide.html) data repository.

Then, to obtain the weather risk index, a linear combination of the wind risk index and the water deficit risk index has been carried out assigning the following relative weights:

$$WRI = 0.6 \cdot WNRI + 0.4 \cdot WDRI \qquad \text{(Eq.5)}$$

1.2.1.2. Historic Risk Index

The other factor obtained to determine the fire risk index is the historic risk index. The historic risk index reflects the probability of a forest fire occurring as a function of the historical recurrence or frequency of fires for each point of the territory.

The risk classification that has been established for the calculation of historic risk is shown in the table below.

Table 6. Risk classification by historical recurrence of forest fires.

Number of forest fires	Classification	Index value
0	Very low	1
1	Low	2
2	Medium	3
3 – 4	High	4
> 5	Very high	5

For Sierra Nevada and Sierra de las Nieves National Parks, the forest fire recurrence data were downloaded from the Andalusian Environmental Information Network (https://portalrediam.cica.es/geonetwork/static/api/records/d0624371-78d7-4e89-b9ef-8e76a294bc97) and provided by the Andalusian Fight-Fighting Service. For El Teide National Park, we obtained this information through the MODIS Fire_cci Burned Area pixel product version 5.1 (Chuvieco et al., 2018). This product contains a monthly global ~250m spatial resolution dataset with information on burned area as well as ancillary data. We accessed this data through the google earth engine (GEE) code editor (https://code.earthengine.google.com/).

1.2.2. Aridity Index

Knowledge of aridity is needed to explain landscape characteristics and the rational utilisation of water resources in many regions. Aridity has been defined in various ways, often using factors based on temperature and precipitation. We applied the widely used Agnew (1993) classification system (Table 7) for climatic aridity zone classification (Proutsos et al., 2021). The classification was applied on the water deficit data generated in the previous section (see Section 1.2.1.1).

Table 7. Aridity Index (AI) threshold values for climatic aridity zone classification according to Agnew (1993).

Water deficit ranges (mm)	Classification	Index value
> 1.08	Hyper-arid	5
1.08 – 0.81	Arid	4
0.81 – 0.63	Semi-Arid	3
0.63 – 0.45	Sub-humid	2
< 0.45	Humid	1

Unit: dimensionless

1.2.3. Pest and Disease Hazard

In this study, we assessed pest and disease incidence using data from the Spanish National Forest Inventory (IFN) and the Spanish ICP network, a large scale systematic monitoring network established on a 4 × 4 km virtual grid projected over the Spanish National Park network as complementary to de European ICP.

In both datasets the different pathogens present in the plot have been identified and an estimate of damage has been provided. To synthesize these two critical components into

a comprehensive measure, we constructed the Pest and Disease Hazard index. This composite index provides a balanced representation of the dual threats posed by both the abundance of pathogens (NP) and the severity of their impact (DS). The index was calculated by assigning equal weight (50-50) to the number of detected pathogens and the damage assessment, ensuring a holistic evaluation of the overall pest and disease risk within each plot.

Since in both datasets the level of detail with which the different pathogens have been identified is different, they have been grouped into 3 classes:

- Fungi
- Insects
- Epiphytic plants

A value of 1 is then assigned to each class and a sum is calculated. Thus, when the variable has a value of 3 (maximum value) it means that pathogens of all 3 classes are present on the plot. For the severity of damage, the ICP network establishes a severity category ranging from 1 to 5, in the case of IFN3 from 1 to 3.

Finally, to calculate the composite index, both variables were rescaled between 0 and 1 to obtain a standardised pest and disease hazard index. The equation for the calculation of the index is shown below:

$$PDHI = 0.5 \cdot NP + 0.5 \cdot DS \quad \text{(Eq.6)}$$

Unit: dimensionless

We used the inverse distance weighting (IDW) to predict the value of the variable at an unsampled locations from the value of the variable at various sampled points.

We obtained the raw data of the second and third Spanish National Forest Inventory (IFN2 and IFN3; 1987 - 2007) in CSV format from the MITECO data repository (https://www.miteco.gob.es/es/biodiversidad/temas/inventarios-nacionales/inventario-forestal-nacional.html). The ICP Forests data Level I set in National Parks were obtained from (http://www.icp-forests.net). These data were evaluated once annually from 1986 to 2020.

1.2.4. Forest continuity

Forest continuity influence fire behaviour and severity by promoting high vertical and horizontal fuel continuity (Lecina-Diaz et al., 2014), whereas forest gaps can give opportunities for fire suppression (Mitsopoulos et al., 2016). Thus, we calculated the proportion of forest around each pixel (500 m), as a measure of forest continuity (ICF). For this, we converted the forest map of Spain into a binary raster layer where 1 corresponds to pixels classified as forest land and 0 to non-forest land. Next, a neighbourhood is defined, which represents the spatial connectivity of each pixel. In this case, a 3x3 matrix is used that considers the connectivity of the surrounding pixels. We then calculate the sum of the neighbourhood connectivity values for each pixel by summing the 8 neighbouring pixels. Thus, a value of 9 (maximum value) indicates that in the 3 x 3-pixel matrix all pixels are forest land. The equation for the calculation of the index is shown below:

$$ICF(i,j) = \frac{\sum_{a=-1}^{1}\sum_{b=-1}^{1} R(i+a, j+b)}{9} \quad \text{(Eq.7)}$$

Where:

- $R(i,j)$ is the pixel value in the (i,j) position
- (a,b) are indices that traverse the values in the neighbourhood (-1,0,1)
- $\sum_{a=-1}^{1}\sum_{b=-1}^{1} R(i+a, j+b)$ represents the connectivity function that sums the values of the pixels in the neighbourhood around the central pixel
- 9 is the total number of pixels in the neighbourhood (3x3)

Finally, the result is normalised by dividing by the total number of neighbours to obtain a continuity index on a scale of 0 to 1.

Unit: dimensionless

We obtained the raw data of the Spanish Forest Map (SFM) in shapefile format from the MITECO data repository (https://www.miteco.gob.es/es/cartografia-y-sig/ide/descargas/biodiversidad/mfe.html).

1.2.5. Distance to roads

We measured the minimum distance from each pixel (since pixel centroid) to the nearest communication route (roads or paths).

Unit: kilometers

We obtained thematic cartography (administrative boundaries, roads) produced by MITECO (https://www.miteco.gob.es/es/cartografia-y-sig/ide.html).

1.2.6. Population density

We obtained the population density layer in shapefile format for each municipality in Spain provided by MITECO (https://www.miteco.gob.es/es/cartografia-y-sig/ide.html). We then rasterise this layer by assigning to each pixel the population density of the municipality to which it corresponds.

Unit: Number of inhabitants (hab)/km^2

1.3.Susceptibility

1.3.1. Fuel load

The most frequently used fire fuel attributes are structure (vertical and horizontal) and fuel load (biomass) (Arroyo et al., 2008). Biomass is needed to estimated forests fuel loads. In this work, fuel load was computed from tree and shrub biomass (aboveground)

of each live individual in each IFN3 plots, that were computed from dendrometric variables (dbh, canopy cover, height) using species-specific allometric equations developed by Montero et al. (2005) and González et al. (2020). We then summarized to obtain the total biomass of each plot:

$$BtotIFN3 = \sum_{i=1}^{n} m_i \quad \text{(Eq.8)}$$

Where:

- $BtotIFN3$ is the total biomass of the plot
- n is the number of individuals in the plot
- mi is the biomass of the i-th individual

Unit: tons/ha

We used the inverse distance weighting (IDW) to predict the value of the variable at an unsampled locations from the value of the variable at various sampled points.

We obtained the raw data of the third Spanish National Forest Inventory (IFN3; 1997 - 2007) in CSV format from the MITECO data repository (See section 1.1 for a full description of the data).

1.3.2. Vertical forest continuity

Vegetation structural complexity has a great influence on fire severity (Domingo et al., 2021). The presence of a continuous vertical layer of vegetation, formed as both a shrub layer and tree cover facilitates fire transition from the surface to tree crown (Moinuddin and Sutherland, 2020). Depending on fire conditions, such as topography or wind intensity, vegetation vertical continuity can lead to an energetic behaviour of the flame front, which prevents its extinction from land or air (Calvo et al., 2023).

Here, vegetation structural complexity has been analysed in terms of diversity with an adaptation of the method proposed by Shannon, (1948). This index expresses the level of vegetation homogeneity in the vertical distribution of vegetation layers.

$$VFC = -\sum_{i=1}^{S} p_i \cdot log_2(p_i) \quad \text{(Eq.9)}$$

Where:

- VFC is the vertical forest continuity of the plot
- S is the number of vegetation layers in the plot
- pi is the proportion of individuals of layer i relative to the total number of individuals.

This index takes into account both layers richness (the number of vegetation layers) and evenness (the relative distribution of individuals among layers) in each plot. The base of

the logarithm (log_2) determines the unit of measurement for Shannon entropy, and a base of 2 is commonly used to express the information in bits.

We classified IFN3 plots into vertical layers of 0.5 meters. We then counted the number of individuals in each of these strata using the height value.

Unit: dimensionless

We used the inverse distance weighting (IDW) to predict the value of the variable at an unsampled locations from the value of the variable at various sampled points.

We obtained the raw data of the third Spanish National Forest Inventory (IFN3; 1997 - 2007) in CSV format from the MITECO data repository (See section 1.1 for a full description of the data).

1.3.3. Leaf Area Index

Leaf Area Index will affect forest susceptibility to drought (Jump et al., 2017). All available MCD15A3H time series images, covering the study areas between 2002 – 2007 (summer months), were used to obtain a good estimate of LAI. The MCD15A3H Version 6.1 Moderate Resolution Imaging Spectroradiometer (MODIS) Level 4, is a 4-day composite LAI data set with 500 meter pixel size.

Units: m^2/m^2

This product was downloaded with Google Earth Engine (https://earthengine.google.com/).

1.3.4. Flammability

The relationship between plant traits and flammability at species level is important for a broader understanding of the vegetation-fire dynamic at the local and landscape scales. Tree species differ in regard to flammability, and many plant functional traits contribute to flammability at species, community and vegetation level (Popović et al., 2021).

We classify the different species according to 4 levels of flammability (Table 8), following the criteria of Elvira and Hernando, (1989):

Table 8. Species classification by flammability characteristics.

Description	Classification	Index value
Low flammable species	Very low	1
Medium flammable species	Low	2
Highly flammable species during summer	Medium	3
Highly flammable species almost all year round	High	4

We then calculated the percentage contribution of each species to the total biomass of the national forest inventory plots (IFN3; see Section 1.3.1. Fuel load). Once the percentages were obtained, we performed a weighted sum at plot level using the ranking values in Table 8 (Eq. 10).

$$Flam = \sum_{i=1}^{n} pbiomass_i \cdot flammability_i \quad \text{(Eq.10)}$$

Where:

- $Flam$ is the total value of flammability of the plot.
- $flammability_i$ is the value of flammability of the i species.
- $pbiomass_i$ is the percentage of biomass of species i relative to the total biomass of the plot.

Unit: dimensionless

We used the inverse distance weighting (IDW) to predict the value of the variable at an unsampled locations from the value of the variable at various sampled points.

1.3.5. Hydraulic traits

We classify the different species according to 5 levels of drought sensitivity (Table 9), following the criteria of Ruiz de la Torre, 2006:

Table 9. Species classification by drought sensitivity.

Description	Classification	Index value
Very low sensitive to drought	Very low	1
Low sensitive	Low	2
Medium	Medium	3
Sensitive	High	4
Very sensitive to drought	Very High	5

We then calculated the percentage contribution of each species to the total biomass of the national forest inventory plots (IFN3; see Section 1.3.1. Fuel load). Once the percentages were obtained, we performed a weighted sum at plot level using the ranking values in Table 9 (Eq. 11).

$$Htraits = \sum_{i=1}^{n} pbiomass_i \cdot droughtsens_i \quad \text{(Eq.11)}$$

Where:

- $Htraits$ is the total value of hydraulic traits of the plot.
- $droughtsens_i$ is the value of drought sensitivity of the i species.
- $pbiomass_i$ is the percentage of biomass of species i relative to the total biomass of the plot.

Unit: dimensionless

We used the inverse distance weighting (IDW) to predict the value of the variable at an unsampled locations from the value of the variable at various sampled points.

1.3.6. Rooting depth

Deep roots may improve water uptake and increase drought resistance of plant species. We classify the different species according to 5 levels of rooting depth (Table 10), following the criteria of Ruiz de la Torre, 2006:

Table 10. Species classification by root depth.

Description	Index value
Taproots	1
Radical tracer system	2
Shallow root system	3
Penetrating radical system	4
Axonomorphic root system	5

We obtained information about the type of root system of each species from the BROT 2.0 database (https://figshare.com/collections/BROT_2_0_A_functional_trait_database_for_Mediterranean_Basin_plants/3843841). The database includes 25,764 individual records of 44 traits from 2,457 plant taxa distributed in 119 taxonomic families. We selected data on vegetative, sexual reproductive and regeneration traits (Tavşanoğlu and Pausas, 2018).

We then calculated the percentage contribution of each species to the total biomass of the national forest inventory plots (IFN3; see Section 1.3.1. Fuel load). Once the percentages were obtained, we performed a weighted sum at plot level using the ranking values in Table 10 (Eq. 12).

$$Rdepth = \sum_{i=1}^{n} pbiomass_i \cdot rootdepth_i \quad \text{(Eq.12)}$$

Where:

- $Htraits$ is the total value of hydraulic traits of the plot.
- $droughtsens_i$ is the value of drought sensitivity of the i species.
- $pbiomass_i$ is the percentage of biomass of species i relative to the total biomass of the plot.

Unit: dimensionless

We used the inverse distance weighting (IDW) to predict the value of the variable at an unsampled locations from the value of the variable at various sampled points.

1.3.7. Suppression difficulty index

The capacity of firefighters to extinguish fire was defined by the Suppression Difficulty Index. The SDI is a multicriteria evaluation tool developed by a former incident commander with more than 25 years of wildfire experience that relies on expert judgement to rescale all sub-index values from 1 to 10 and combines them into an overall dimensionless index where higher values indicate higher suppression difficulty (Silva et al., 2020). The SDI equation is calculated as follows:

$$SDI = I_{tce} / \ I_a + I_m + I_p + I_{ar} + I_c \quad \text{(Eq.13)}$$

Where:

- I_{tce} is the total energy behaviour sub-index.
- I_a is the accessibility sub-index.
- I_m is the mobility sub-index.
- I_p is the penetrability sub-index.
- I_{ar} is the aerial resources sub-index.
- I_c is the fireline construction sub-index.

This provides a simple yet useful summary index that can be mapped across landscapes and its sub-indices can be deconstructed and mapped individually.

Unit: dimensionless

1.3.7.1. Energy behaviour sub-index

The energy behaviour sub-index uses heat per unit area values weighted proportionally by fuel abundance at the pixel scale within a unit of analysis. Here, we simplified the calculation of this index by applying a calorific value index to the biomass content of each pixel. The fire load is defined as the weight of biomass per unit area (kg/ha) capable of developing an amount of heat equivalent to that of the materials contained in the fire sector. In the professional sector, biomass is assigned a reference calorific value of 4400 Kcal/kg:

$$I_{tce} = \ BtotIFN3 \cdot 4400 \quad \text{(Eq.14)}$$

Where $BtotIFN3$ is the fuel load (biomass; kg) of the plot (see section 1.3.1).

Unit: Kcal

We used the inverse distance weighting (IDW) to predict the value of the variable at an unsampled locations from the value of the variable at various sampled points.

1.3.7.2. Accesibility sub-index

This sub-index represents the density of road network available for accessing forest areas to suppress forest fire (Silva et al., 2014). It is computed as an assigned weight depending on the length (m) of the access road network per pixel (Table 11).

Table 11. Assigned weights for elaboration of the accessibility and mobility sub-indices.

Length (m)	Weight
0-100	1
101-200	2
201-300	3
301-400	4
401-500	5
501-600	6
601-700	7
701-800	8
801-900	9
>901	10

Unit: dimensionless

We obtained thematic cartography (roads and paths) produced by MITECO (https://www.miteco.gob.es/es/cartografia-y-sig/ide.html).

1.3.7.3. Mobility sub-index

Mobility refers to the access capacity the forest area provides through the existing fire prevention firebreaks network (Silva et al., 2014). The mobility sub-index is computed as a weight assigned as function of the length of existing fire prevention firebreaks in each pixel (Table 11).

Unit: dimensionless

Information obtained from satellite images and aerial photos.

1.3.7.4. Penetrability sub-index

This sub-index represents the difficulty for firefighters to access the forest area on foot (Silva et al., 2014). The penetrability sub-index is composed of a number of variables such as slope, the shallow soil structure in relationship to its hardness (loose or compact soil), existing fuel density, hill slope aspect and pre-suppression trails (Eq. 15).

$$I_p = \sum \left[\frac{s_i \times d_i \times sh_i + e_i}{pt_i} \right] \times \frac{A_i}{A_t} \qquad \text{(Eq.15)}$$

Where:

- s_i is the weight assigned to the percentage slope of the pixel i.
- d_i is the weight assigned to the difficulty caused by pixel i for firefighters to walk in the area (Table 12).
- sh_i is the weight assigned to soil hardness (Table 12).
- e_i is the weight assigned to the fuel model i slope aspect (Table 12).
- pt_i is the weight assigned to existing pre-suppression trails (Table 12).

Table 12. Assigned values for elaboration of the penetrability sub-index and the adjustment coefficient depending on the slope for the fire-line construction sub-index.

Soil hardness	Slope (%)	Aspect	Pre-extinction trails (m/ha)	Assigned value	Adjustement coefficient
Hard	0-5	N	0-5	10	1
	6-10	-	6-10	9	1
	11-15	NE	11-15	8	1
Moderately hard	16-20	NW	16-20	7	0.8
	21-25	E	21-25	6	0.8
Moderately loose	26-30	W	26-30	5	0.8
	31-35	SE	31-35	4	0.6
	36-40	SW	36-40	3	0.6
	41-45	S	41-45	2	0.6
Loose	>46	-	>46	1	0.5

Unit: dimensionless

We obtained the digital slope model available from the national centre for geographic information (https://centrodedescargas.cnig.es/CentroDescargas/catalogo.do?Serie=MDT02). The terrain aspect was calculated from the digital terrain model available in the same web portal. We used soil maps provided by the National Geographic Institute of Spain (IGN). Additional information was obtained from satellite images or aerial photos.

1.3.7.5. Aerial resources sub-index

This includes three variables related to the different type of aerial resources used in fire suppression (Table 13).

Table 13. Assigned weights for elaboration of the aerial resources sub-index.

Flying time between drops (min)			Assigned weight
Helicopters	Aircraft		
	Amphibious	Land-based	
<5	<20	<20	10
6-15	21-30	21-40	9
16-25	31-40	41-60	8
26-35	41-50	61-80	7
36-45	51-60	81-100	6
46-55	61-70	101-120	5
56-65	71-80	121-140	4
66-75	81-90	141-160	3
76-85	91-100	161-180	2
>86	>101	>181	1

We assigned a constant value of 8 for all study area based on the expert assessment of the Regional Forest Fire Fighting Plan of Andalusia (INFOCA) and information provided by MITECO.

Unit: dimensionless

1.3.7.6. Fireline opening sub-index

This represents the fireline production rate achieved by hand crews using hand tools and machinery, corrected for the fuel model slope (Silva et al., 2014). We assigned two different weights based on the experience of INFOCA's expert firefighting personnel: 8 in the protection buffer of the national park (natural park) and 4 inside the national park boundaries.

1.4. Lack of Adaptative Capacity

1.4.1. Resprouting capacity

The capacity of forests to recover after a wildfire depends on their regeneration capacity, which is based in resprouting capacity and seeding capacity (Lecina-Diaz et al., 2014). Resprouting capacity is defined as the average proportion of adult plants that resprout as percentage, comprising 5 categories (Table 14).

Table 14. Species classification by resprouting capacity.

Description	Index value
No resprouting	1
Limited resprouting	2
Optional resprouting	3
Preferential resprouting	4
Compulsory resprouting	5

We obtained information about the resprouting capacity of each species from the BROT 2.0 database (https://figshare.com/collections/BROT_2_0_A_functional_trait_database_for_Mediterranean_Basin_plants/3843841) and conducted a literature search to complete the species without information.

We then calculated the percentage contribution of each species to the total biomass of the national forest inventory plots (IFN3; see Section 1.3.1. Fuel load). Once the percentages were obtained, we performed a weighted sum at plot level using the ranking values in Table 14 (Eq. 16), being an estimate of the resprouting capacity at the plot level.

$$Resprout = \sum_{i=1}^{n} pbiomass_i \cdot rescap_i \quad \text{(Eq.16)}$$

Where:

- $Resprout$ is the total value of resprouting capacity of the plot.
- $rescap_i$ is the value of resprouting capacity of the i species.
- $pbiomass_i$ is the percentage of biomass of species i relative to the total biomass of the plot.

Unit: dimensionless

We used the inverse distance weighting (IDW) to predict the value of the variable at an unsampled locations from the value of the variable at various sampled points.

1.4.2. Seeding capacity

Seeding capacity refers to the amount of seed available for regeneration after a disturbance and the type of seeds bank, grouped in 5 categories from 1 to 5 (Table 15).

Table 15. Species classification by seeding capacity.

Description	Index value
Without bank	1
Scarce bank in the soil	2
Abundant bank in the soil	3
Abundant bank in the soil and air bank	4
Abundant bank in the soil and in the air bank	5

We obtained information about the seeding capacity of each species from the BROT 2.0 database (https://figshare.com/collections/BROT_2_0_A_functional_trait_database_for_Mediterranean_Basin_plants/3843841) and conducted a literature search to complete the species without information.

We then calculated the percentage contribution of each species to the total biomass of the national forest inventory plots (IFN3; see Section 1.3.1. Fuel load). Once the percentages were obtained, we performed a weighted sum at plot level using the ranking values in Table 15 (Eq. 17), being an estimate of the seeding capacity at the plot level.

$$Seed = \sum_{i=1}^{n} pbiomass_i \cdot seedcap_i \quad \text{(Eq.17)}$$

Where:

- $Seed$ is the total value of seeding capacity of the plot.
- $seedcap_i$ is the value of seeding capacity of the i species.
- $pbiomass_i$ is the percentage of biomass of species i relative to the total biomass of the plot.

Unit: dimensionless

We used the inverse distance weighting (IDW) to predict the value of the variable at an unsampled locations from the value of the variable at various sampled points.

1.4.3. Evapotranspiration

The local climate will determine forest recovery after disturbances (eg. wetter conditions usually facilitate recovery in dry regions). We used the raster files generated in the previous section (see Section 1.2.1.1).

Unit: mm

1.4.4. Solar radiation

Since insolation and solar radiation generate differences (spatial and temporal) in energy and water balances, which in turn are associated with various micro-environmental factors such as humidity and temperature, they can influence the spatial distribution of vegetation. Solar radiation information was extracted from the WorldClim-Global Climate Database (Fick and Hijmans, 2017) (https://worldclim.org). The dataset was downloaded globally at 2.5 arc-min spatial resolution (~ 5 × 5 km at the equator).

Unit: $kJ/m^2/day$

1.4.5. Slope

Topography will also determine forest recovery after disturbances. When the vegetation is destroyed but the soil is left intact, recovery can occur very quickly, as fragments of the original plants remaining can sprout again and new plants can also arise from dormant seeds (Bradshaw, 1997). If the soil is degraded, plant colonization and forest recovery are much more difficult. Bradshaw, (1997) recognized the slope as one of the main limitation topography factors for vegetation recovery.

We used the digital slope model available from the national centre for geographic information (see Section 1.2.1.1).

Unit: %

1.4.6. Forest management

Some external human-related factors can influence the capacity of forest recovery after disturbances. In the case of wildfires and pests and disease outbreaks, forest management will accelerate regeneration of certain species. Three forest management scenarios were generated following Simon and Ameztegui, (2022) which can be projected into a specific plan of forest management (detailing the age of each intervention, and the type - regeneration, improvement - and weight of each one, as detailed in López et al., (2008) and Navarro-Cerrillo et al. (2021). The first scenario, called “low intervention”, foresees short rotations (80 years) and “occasional” thinning actions, promoting the use of wood as biomass. The second scenario, called “traditional silviculture”, seeks the promotion of products of long useful life (structural wood, furniture), which implies extending rotations over 100 years, and implement a selective thinning regime intensity (~30% of basal area). The third scenario, "reduction of climate vulnerability" seeks to improve the adaptation

of the forests to expected future water scarcity through early and heavy thinning (~50% of basal area). As mentioned above, the vegetation in the buffer zones of the three National Parks is dominated by pine forests plantations. In these forest types, a transition towards mixed-species and uneven-aged forests would facilitate rising to one of the main challenges that forest management faces: to develop a climate-smart forestry that contributes to the mitigation of and adaptation to global change (Vadell et al., 2022). Thus, we applied the three forest management scenarios only on stands composed of pine forests plantations. To identify the area covered by these types of formations in each natural area, we used the Spanish Forest Map (SFM). Scenarios were applied by applying percentage reductions on total biomass.

Unit: dimensionless

1.5. Climatic scenarios

We extracted information about the climatic scenarios from the Coupled Model Intercomparison Project Phase 6 (CMIP6, https://pcmdi.llnl.gov/CMIP6/) to assess projected changes in future climate and their impact on the ecosystem service evaluated. To provide plausible future scenarios for management, we selected two contrasting SSPs scenarios (i.e., SSP126 and SSP585), and the two first periods (i.e., 2021–2040, 2041–2060). We then used this information to calculate future projections of aridity and fire risk indices, and evapotranspiration, which affect the Hazard Magnitude and LAC components, respectively. We did not assess projected trends for other indicators related hazards (e.g., pest and disease outbreaks) to avoid an excessive complex analysis.

2. Weighting and aggregating the indicators

All factors were standardized to obtain a range from 0 to 1. The standardization has been carried out by means of the following expression:

$$x' = (x - \mu)/\sigma \quad \text{(Eq.18)}$$

Where:

- x' is the standardized value
- x is the original value
- μ is the sample mean
- σ is the sample standard deviation

Next, we applied statistical weights based on expert weights and analytic hierarchy process (AHP) to determine the global ranking score of each indicator of the risk components (Saaty and Vargas, 2012). To check the consistency of the decision making and reduce the bias in the process, a consistency ratio (CR) was obtained with Equations (19) and (20).

$$CR = CI/RI \quad \text{(Eq.19)}$$

$$CI = (\lambda max - n)/(n - 1) \quad \text{(Eq.20)}$$

Where:

- CR is the consistency ratio
- CI is the consistency index
- RI is the random index
- λmax is the maximum value in the average of dividing the sum of the weights
- n is the number of criteria

CR values of 0.10 and lower are considered tolerable (Saaty and Vargas, 2012). Results of the weights for experts' weights and AHP are given in Table 16.

Table 16. Weight for each indicator.

Component	Indicators	Weights
Hazard magnitude	Fire Risk Index	0.242
	Aridity Index	0.277
	Pest and Disease Hazard	0.086
	Forest continuity	0.056
	Distance to roads	0.174
	Population density	0.165
Susceptibility	Fuel load	0.29
	Vertical forest continuity	0.08
	Leaf Area Index	0.11
	Flammability	0.07
	Hydraulic traits	0.10
	Rooting depth	0.14
	Suppression Difficulty Index	0.21
Lack of Adaptative Capacity	Resprouting capacity	0.22
	Seeding capacity	0.17
	Evapotranspiration	0.12
	Solar radiation	0.10
	Slope	0.07
	Forest management	0.32

Afterwards, we aggregate the indicators by summing them:

$$\begin{aligned} Hazard\ magnitude\ (HM) &= (0.242 \cdot Fire\ risk\ index) + (0.277 \cdot Aridity\ risk) \\ &+ (0.086 \cdot Pest\ and\ disease\ hazard) \\ &+ (0.056 \cdot Forest\ continuity) \\ &+ \big(0.174 \cdot (1 - Distance\ to\ roads)\big) \\ &+ (0.165 \cdot Population\ density) \end{aligned} \quad \text{(Eq.21)}$$

$$
\begin{aligned}
&Susceptibility\ (S) \\
&\quad = (0.29 \cdot Fuel\ load) + (0.08 \cdot Vertical\ forest\ continuity) \\
&\quad + (0.11 \cdot Leaf\ area\ index) + (0.07 \cdot Flammability) \\
&\quad + (0.10 \cdot Hydraulic\ traits) + (0.14 \cdot (1 - Rooting\ depth)) \\
&\quad + (0.21 \cdot Supression\ difficulty\ index)
\end{aligned}
\tag{Eq.22}
$$

$$
\begin{aligned}
&Lack\ of\ adaptative\ capacity\ (LAC) \\
&\quad = 1 - ((0.22 \cdot Resprouting\ capacity) + (0.17 \cdot Seeding\ capacity) \\
&\quad + (0.12 \cdot (1 - Evapotranspiration)) \\
&\quad + (0.10 \cdot (1 - Solar\ radiation)) + \big(0.07 \cdot (1 - Slope)\big) \\
&\quad + (0.32 \cdot Forest\ management))
\end{aligned}
\tag{Eq.23}
$$

Finally, combined the components by following the Equation 24:

$$Risk = \ E \ \cdot HM^{S} \cdot LAC \tag{Eq.24}$$

REFERENCES

Agnew, C., 1993. World atlas of desertification: United Nations Environment Programme. London: Edward Arnold, 1992. 69 pp.

Arroyo, L.A., Pascual, C., Manzanera, J.A., 2008. Fire models and methods to map fuel types: The role of remote sensing. For. Ecol. Manag. 256, 1239–1252.

Bradshaw, A.D., 1997. The importance of soil ecology in restoration science. Restor. Ecol. Sustain. Dev. 33–64.

Calvo, R.C., Varo Martínez, M.Á., Ruiz Gómez, F., Ariza Salamanca, A.J., Navarro-Cerrillo, R.M., 2023. Improvements of Fire Fuels Attributes Maps by Integrating Field Inventories, Low Density ALS, and Satellite Data in Complex Mediterranean Forests. Remote Sens. 15, 2023. https://doi.org/10.3390/rs15082023

Chuvieco, E., Pettinari, M.L., Lizundia-Loiola, J., Storm, T., Padilla Parellada, M., Initiative, E.F.C.C., 2018. MODIS Fire_cci burned area pixel product, version 5.1. Cent. Environ. Data Anal. 1, 943–956.

Domingo, D., Lamelas, M.T., García, M.B., 2021. Characterization of vegetation structural changes using multi-temporal LiDAR and its relationship with severity in Calcena wildfire.

Elvira, L.M., Hernando, C., 1989. Inflamabilidad y energía de las especies de sotobosque. Monogr. INIA 68, 99.

Fick, S.E., Hijmans, R.J., 2017. WorldClim 2: new 1-km spatial resolution climate surfaces for global land areas. Int. J. Climatol. 37, 4302–4315. https://doi.org/10.1002/joc.5086

González, G.M., Leiva, C.L., Ruiz-Peinado, R., Senespleda, E.L., Onrubia, R., Pasolodos, M., 2020. Producción de biomasa y fijación de carbono por los matorrales españoles y por el horizonte orgánico superficial de los suelos forestales. Ministerio de Agricultura, Pesca y Alimentación, Secretaría General Técnica.

Hamon, W.R., 1963. Estimating Potential Evapotranspiration. Trans. Am. Soc. Civ. Eng. 128, 324–338. https://doi.org/10.1061/TACEAT.0008673

Jump, A.S., Ruiz-Benito, P., Greenwood, S., Allen, C.D., Kitzberger, T., Fensham, R., Martínez-Vilalta, J., Lloret, F., 2017. Structural overshoot of tree growth with climate variability and the global spectrum of drought-induced forest dieback. Glob. Change Biol. 23, 3742–3757. https://doi.org/10.1111/gcb.13636

Lecina-Diaz, J., Alvarez, A., Retana, J., 2014. Extreme Fire Severity Patterns in Topographic, Convective and Wind-Driven Historical Wildfires of Mediterranean Pine Forests. PLOS ONE 9, e85127. https://doi.org/10.1371/journal.pone.0085127

Lecina-Diaz, J., Martínez-Vilalta, J., Alvarez, A., Banqué, M., Birkmann, J., Feldmeyer, D., Vayreda, J., Retana, J., 2021. Characterizing forest vulnerability and risk to climate-change hazards. Front. Ecol. Environ. 19, 126–133. https://doi.org/10.1002/fee.2278

López, E., Climent, J.M., Montero, G., 2008. Selvicultura de Pinus canariensis Sweet. Compend. Selvicultura Apl. En Esp. INIA Madr.

Mitsopoulos, I., Mallinis, G., Paschalidou, A., Emmanouloudis, D., 2016. Fire suppression difficulty estimation and mapping in a Mediterranean landscape using Landsat-8 imagery and spatial fire behavior analysis, in: 2016 18th Mediterranean Electrotechnical Conference (MELECON). IEEE, pp. 1–6.

Moinuddin, K.A.M., Sutherland, D., 2020. Modelling of tree fires and fires transitioning from the forest floor to the canopy with a physics-based model. Math. Comput. Simul. 175, 81–95.

Montero, G., Ruiz-Peinado, R., Munoz, M., 2005. Producción de biomasa y fijación de CO2 por los bosques españoles. INIA-Instituto Nacional de Investigación y Tecnología Agraria y Alimentaria ….

Natural evaporation from open water, bare soil and grass, 1948. . Proc. R. Soc. Lond. Ser. Math. Phys. Sci. 193, 120–145. https://doi.org/10.1098/rspa.1948.0037

Popović, Z., Bojović, S., Marković, M., Cerdà, A., 2021. Tree species flammability based on plant traits: A synthesis. Sci. Total Environ. 800, 149625. https://doi.org/10.1016/j.scitotenv.2021.149625

Proutsos, N.D., Tsiros, I.X., Nastos, P., Tsaousidis, A., 2021. A note on some uncertainties associated with Thornthwaite's aridity index introduced by using different potential evapotranspiration methods. Atmospheric Res. 260, 105727.

Rothermel, R.C., 1972. A mathematical model for predicting fire spread in wildland fuels. Intermountain Forest & Range Experiment Station, Forest Service, US ….

Saaty, T.L., Vargas, L.G., 2012. Models, methods, concepts & applications of the analytic hierarchy process. Springer Science & Business Media.

Shannon, C.E., 1948. A mathematical theory of communication. Bell Syst. Tech. J. 27, 379–423.

Silva, F.R. y, O'Connor, C.D., Thompson, M.P., Martinez, J.R.M., Calkin, D.E., 2020. Modelling suppression difficulty: current and future applications (vol 29, pg 781, 2020). Int. J. WILDLAND FIRE 29, 752–752.

Simon, D.C., Ameztegui, A., 2022. Influence of thinning intensity and frequency on the provision of ecosystem services in Mediterranean mountain pine forests under climate change scenarios.

Tavşanoğlu, Ç., Pausas, J.G., 2018. A functional trait database for Mediterranean Basin plants. Sci. Data 5, 1–18.

Thornthwaite, C.W., 1948. An approach toward a rational classification of climate. Geogr. Rev. 38, 55–94.

Vadell, E., Pemán, J., Verkerk, P.J., Erdozain, M., De-Miguel, S., 2022. Forest management practices in Spain: Understanding past trends to better face future challenges. For. Ecol. Manag. 524, 120526.

Vörösmarty, C.J., Federer, C.A., Schloss, A.L., 1998. Potential evaporation functions compared on US watersheds: Possible implications for global-scale water balance and terrestrial ecosystem modeling. J. Hydrol. 207, 147–169.

y Silva, F.R., Martínez, J.R.M., González-Cabán, A., 2014. A methodology for determining operational priorities for prevention and suppression of wildland fires. Int. J. Wildland Fire 23, 544–554.